Cerebrospinal fluid flow into the spinal cord in a rat model of extradural constriction: a network of perivascular pathways

Joel Anthony Berliner

MACQUARIE University
SYDNEY·AUSTRALIA

A Thesis submitted for the partial fulfilment of the requirements for the degree of Master of Research in the Faculty of Medicine and Health Sciences.

Cerebrospinal fluid flow into the spinal cord in a rat model of extradural constriction: a network of perivascular pathways

Joel Anthony Berliner

43905447

A Thesis submitted for the partial fulfilment of the requirements for the degree of Master of Research in the Faculty of Medicine and Health Sciences.

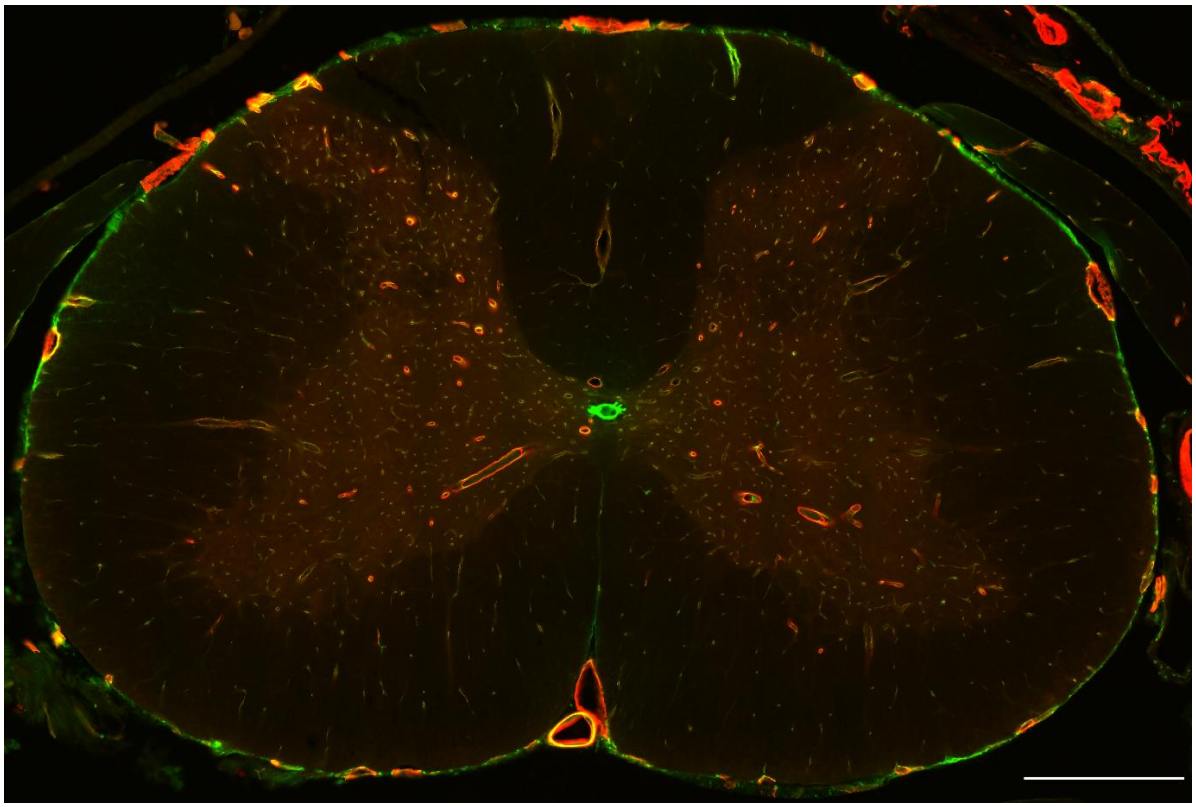

Cervical cross-section of a rat spinal cord with fluorescent CSF tracer (green) and blood vessels labelled.

Supervisor: Professor Marcus Stoodley[1]; Co-supervisor: Dr Sarah Hemley[1]

Key words: Cerebrospinal Fluid; Perivascular Spaces; Spinal Cord; Fluid Inflow; CSF Tracer; CSF Physiology; Subarachnoid Space Obstruction; Syringomyelia.

Word count: 9421
Abstract: 356
Figures: 9

[1]Department of Clinical Medicine, Faculty of Medicine and Health Sciences, Macquarie University, Sydney, NSW, Australia.

Declaration of originality

I certify that the work in this thesis entitled "Cerebrospinal fluid flow into the spinal cord in a rat model of extradural constriction: a network of perivascular pathways", has not previously been submitted for a degree nor has it been submitted as part of requirements for a degree to any other university or institution other than Macquarie University. I also certify that the thesis is an original piece of research and it has been written by me. Any help and assistance that I have received in my research work and the preparation of the thesis itself have been appropriately acknowledged. In addition, I certify that all information sources and literature used are indicated in the thesis. The research presented in this thesis was approved by the Animal Care and Ethics Committees of Macquarie University, ARA 2012/008.

Joel Anthony Berliner

43905447

10/10/2016

Conflict of interest statement

The research was conducted in the absence of any commercial or financial relationships that could be construed as a potential conflict of interest.

Declaration of contribution

The experiment was designed by Professor Marcus Stoodley, Dr Sarah Hemley, Professor Lynne Bilston, Dr Elmira Najafi, and Dr Thomas Woodcock. The surgical procedures, including the creation of the subarachnoid space constriction model, the cisterna magna injections and intracardiac perfusions were carried out by Dr Elmira Najafi. Dr Elmira Najafi and Dr Thomas Woodcock undertook post-operative care of the animals. Following, Dr Thomas Woodcock cryoprotected and embedded the spinal cord segments in OCT. All consecutive procedures, data acquisition and analysis were performed by the author of this paper.

Acknowledgements

First and foremost, I would like to acknowledge the entire Neurosurgery Team at Macquarie University for welcoming me with open arms and making my tuition such a pleasurable and enriching experience. The Master of Research experience would not have been the same without all of your support.

To my supervisor Professor Marcus Stoodley, your research wisdom and passion have been inspiring. Thank you for accepting me so willingly into your team and for your patience. Your tutelage and the knowledge you have imparted has been invaluable. I look forward to continuing learning from you and growing as a researcher under your mentorship.

To my co-supervisor Dr Sarah Hemley, thank you for confidence and unwavering guidance throughout this research project. You have encouraged and nurtured me in my work and have been diligent in keeping me on task and on track. Thank you for your insights and your patience with my questions. I could not have picked a better or more thoughtful teacher leading me into a career in research. My deepest gratitude.

Dr Magdalena Lam, thank you for communicating your research experience so fruitfully and without hesitation. I have been humbled to learn from you and have been inspired by your drive for the acquisition of knowledge.

I'd like to give special thanks to my colleagues and friends who proofed this thesis.

To the lab operations managers in the Department of Biomedical Sciences, Ms Lucy Lu, Ms Tamara Leo, Ms Louise Marr, thank you for your support and your due diligence in ensuring all equipment was functional and chemicals were in stock.

Finally to my family and dear friends who have supported me through this experience and provided me with constant love, affection, understanding and, not to forget, sustenance, your part in this means more to me than words can describe. From the bottom of my heart, thank you.

Table of contents

Declaration of originality 1

Conflict of interest statement 2

Declaration of contribution 3

Acknowledgements 4

Abstract 6

Introduction 7

Materials and methods 10

Spinal cord constriction surgery 10

CSF tracer injection 11

Immunohistochemistry 12

Microscopic image acquisition 13

Image analysis 13

Statistical analysis 13

Results 15

1 week post-surgery 15

Distribution of CSF tracer in the spinal cord 15

Distribution of CSF tracer associated with blood vessels 16

6 weeks post-surgery 17

Distribution of CSF tracer in the spinal cord 17

Distribution of CSF tracer associated with blood vessels 21

Discussion 27

Limitations 32

Conclusion 33

References 34

Abstract

The understanding of how cerebrospinal fluid (CSF) flows in and around central nervous system (CNS) tissue remains somewhat elusive. Historically, CSF was thought to flow around and within set structural boundaries of the CNS. More recently, a dynamic flow and exchange within neural tissue has been revealed. Of key interest is the role of perivascular pathways in fluid flow into and out of CNS tissue. In the brain, CSF has been reported to flow into tissue via periarterial pathways and out of tissue via perivenular pathways. The aim of this study was to determine whether the same flow pattern, or a notably different pattern, exists within the spinal cord. A C7 to T1 laminectomy was performed on 28 Sprague-Dawley rats. An extradural suture was tied around the spinal cord to obstruct CSF flow in 16 rats. The remaining animals were used as laminectomy-only controls. At 1 or 6 weeks post-surgery, animals were injected intracisternally with the fluorescent tracer Alexa-Fluor 647 ovalbumin and perfused 10 or 20 min after injection. Fixed and cryoprotected spinal segments were sectioned transversely and immunolabelled for smooth muscle actin and rat endothelial cell antigen. Fluorescent micrographs were taken and the distribution of tracer around arterioles, venules and capillaries was analysed. Intensity of gross grey matter and white matter tracer fluorescence showed that, at the 10 min time-point 6 weeks post-surgery, white matter in constriction animals (n = 5) had a significantly higher fluorescence intensity compared to the laminectomy-only animals (n = 3). Constriction animals in the same experimental group showed distribution of tracer around venules, arterioles and capillaries, whereas the control animals showed equivalent tracer distribution around arterioles and capillaries only. The results of this study suggest that an obstruction to CSF flow in the subarachnoid space may cause both increased fluid flow into the spinal cord and changes to the perivascular inflow pathways. Perivenular and pericapillary pathways, in addition to periarterial pathways, may act as an inflow route for CSF to the spinal cord tissue when the subarachnoid space is obstructed. Knowledge of the mechanics of normal and obstructed CSF physiology is necessary for understanding fluid accumulation pathologies, such as syringomyelia.

Introduction

Cerebrospinal fluid (CSF) holds several functions in the central nervous system (CNS). CSF bathes the spinal cord and brain and fills the cerebral ventricles, acting as a cushion to protect neural tissue from mechanical insult (Brinker *et al.*, 2014). It also functions to regulate neurochemicals, stabilising pH as well as filtering out pathogens and overabundant proteins that can cause neurotoxicity (Simon and Iliff, 2016). CSF is thus critical to the maintenance of CNS homeostasis, although how CSF circulates and exchanges with interstitial fluid (ISF) of the brain and spinal cord is not completely understood.

The classical model of CSF physiology is of secretion, followed by circulation, and then reabsorption. This model describes the active secretion of CSF by the choroid plexus in each ventricle (Cserr, 1971). Bulk flow of CSF is driven by respiration and the pulsatility of cerebral arteries, through the ventricular system and into the subarachnoid space surrounding the brain and spinal cord, via the foramina of Luschka and Magendie (Hladky and Barrand, 2014). From here, CSF is thought to drain into the venous circulation through the arachnoid villi of dural sinuses, into the lympathic circulation via dural lymphatic vessels or by traversing spinal and cranial nerve roots and entering peripheral lymphatics (Cserr, 1971, Hladky and Barrand, 2014, Bedussi *et al.*, 2015, Louveau *et al.*, 2015). Notably, brain and spinal cord tissue lack lympathic vessels, so fluid homeostasis and drainage within the CNS must occur by other means.

Homeostasis of the extracellular fluid compartments of the CNS was classically understood as an exchange between CSF and ISF by diffusion (Davson, 1972, Levin and Sisson, 1972, Milhorat, 1975). The current understanding stipulates a more dynamic system, where CSF and ISF are in constant exchange in CNS tissue along specialised anatomical pathways, the perivascular spaces. Recent research by Iliff *et al.* has demonstrated that fluid enters brain tissue via pathways around penetrating arterioles, known as periarterial spaces (Iliff *et al.*, 2012). Bulk (convective) flow of fluid across the brain tissue is thought to result in the clearance of ISF and solutes via perivenular pathways (Iliff *et al.*, 2012). Alternatively, the work of Carare *et al.* contraindicate this proposed perivenular clearance pathway, demonstrating that drainage of solutes and fluid from the brain tissue of mice occurred via the basement membranes of capillaries and arteries (Carare *et al.*, 2008). Further, it has been reported through mathematical modelling that a reverse clearance mechanism may occur in the perivascular spaces of cerebral capillaries and arterioles, where solutes and fluid traverse the perivascular space against the direction of blood flow (Schley *et al.*, 2006). Still, the expansion of cerebral arteries during cardiac systole has been speculated to drive fluid exchange in perivascular spaces (Iliff *et al.*,

2013). Rapid flow of CSF from the subarachnoid space to perivascular spaces of the brain and spinal cord has been demonstrated to be driven by arterial pulsations (Rennels *et al.*, 1985, Rennels *et al.*, 1990, Stoodley *et al.*, 1997). It is not known whether the described fluid inflow and outflow pathways in the brain are the same in the spinal cord.

Obstructions to CSF flow can result in fluid accumulation within neural tissue. Fluid accumulation can cause cell loss, scar tissue generation, paralysis, with severe cases resulting in death by haemorrhage or respiratory arrest (Tait *et al.*, 2010, Klekamp, 2013, Sakushima *et al.*, 2013). CNS pathologies often caused by fluid flow obstructions include hydrocephalus (Cheng *et al.*, 2007, Cheng and Bilston, 2010, Cheng *et al.*, 2010), oedema (Saadoun and Papadopoulos, 2010, Tait *et al.*, 2010) and syringomyelia (Brodbelt and Stoodley, 2003, Brodbelt *et al.*, 2003a, Bilston *et al.*, 2010).

Syringomyelia is associated with a wide range of conditions that obstruct fluid flow. These conditions include hydrocephalus, Chiari malformations, arachnoiditis, spinal cord trauma and tumours (Stoodley *et al.*, 1999, Brodbelt *et al.*, 2003b, Peraud and Grau, 2009, Kobayashi *et al.*, 2012, Sakushima *et al.*, 2013). From these obstructions to fluid flow, archetypal fluid-filled cysts (syrinxes) form within the spinal cord (Madsen *et al.*, 1994). Obstructions in the spinal subarachnoid space, which occurs in spinal cord trauma, tumours and non-traumatic arachnoiditis, can result in the formation of non-communicating, extracanalicular syrinxes (Stoodley *et al.*, 1997, Brodbelt *et al.*, 2003a, Klekamp, 2013). Even though these conditions are associated with altered CSF flow, it is not known how these obstructions change the dynamics of fluid going into, or out of, the spinal cord tissue or change the pathways by which CSF moves. Understanding the physiology of CSF flow under normal and obstructed conditions may help elucidate the mechanics of abnormal fluid accumulation.

CSF flow pathways cannot be studied in humans using current techniques, so animal models are required. Previous animal models have been implemented to investigate blood-spinal cord barrier permeability, molecular changes in CNS pathologies and qualitative flow of CSF (Schurr *et al.*, 1953, Becker *et al.*, 1972, Torvik and Murthy, 1977, Nakamura *et al.*, 1983, Milhorat *et al.*, 1993, Stoodley *et al.*, 1999, Josephson *et al.*, 2001, Klekamp *et al.*, 2001, Brodbelt *et al.*, 2003a, Brodbelt *et al.*, 2003b). Josephson *et al.* introduced a model of post-traumatic syringomyelia that involved narrowing the spinal subarachnoid space with an extradural suture and obstructing CSF flow (Josephson *et al.*, 2001). In doing so, syrinx formation occurred within 8 to 13 weeks (Josephson *et al.*, 2001). However, no models to date

have assessed the pathways involved in spinal CSF inflow in animals with normal and obstructed subarachnoid spaces.

The current investigation set out to study CSF flow pathways into the spinal cord, with particular focus on changes in perivascular pathways involved when CSF flow in the subarachnoid space was obstructed. Using a subarachnoid space constriction model modified from Josephson *et al.* (Josephson *et al.*, 2001), CSF tracer distribution was compared in normal and obstructed Sprague-Dawley rats at 1 week and 6 weeks post-surgery. The general distribution of tracer within the grey and white matter of the spinal cord was assessed and arterioles, venules and capillaries were identified to examine perivascular flow. It was hypothesised that obstruction to the subarachnoid space would enhance CSF flow into the spinal cord, primarily via increased periarterial flow immediately rostral to the extradural constriction.

Materials and methods

This study was approved by the Animal Care and Ethics Committee of Macquarie University (ARA 2013/047). A population of 28 male Sprague-Dawley rats weighing 300 – 400 g was divided into two groups: experimental animals and control animals. Sixteen experimental animals underwent surgery to constrict the subarachnoid space between spinal levels C7 and T1 and 12 control animals underwent laminectomy-only surgeries. Animals were assigned survival points of 1 or 6 weeks post-surgery, at which time a second surgery was performed to inject the CSF tracer, Alexa-Fluor 647 ovalbumin (OA-647, 45 kD) into the cisterna magna at 10 min or 20 min time points (Table 1).

Table 1. Animal number used for CSF tracer study.

	No. of animals at each survival point			
Experimental group	***1 week***		***6 weeks***	
	10 min	*20 min*	*10 min*	*20 min*
Control	3	3	3	3
Constriction	3	3	5	5

Spinal cord constriction surgery

Aseptic techniques were used in operative fields in all surgical procedures. General anaesthesia was induced with 5% isoflurane in oxygen (1 L/min) and maintained with 2 – 2.5% isoflurane through a nose cone. Animals were placed in a prone position, and the skin was shaved and sterilised with povidone iodine. The cervico-thoracic junction was dissected out and C7 – T1 laminectomies were performed. An extradural suture (nonabsorbable 6-0 polypropylene monofilament, Ethicon, Johnson & Johnson Medical Pacific Pty Ltd, Sydney, Australia) was threaded around the spinal cord following the curve of the vertebral foramen, and tightened until the posterior spinal vein was occluded, and then tied with a reef knot (Figure 1A – C). Absorbable 4-0 Coated Vicryl sutures (Ethicon, Johnson & Johnson Medical Pacific Pty Ltd, Sydney, Australia) were then used to close the wound. Buprenorphine (0.05 mg/kg of

324 µg/mL) in 5% glucose solution was administered subcutaneously at the conclusion of each operation. Further doses were administered as required.

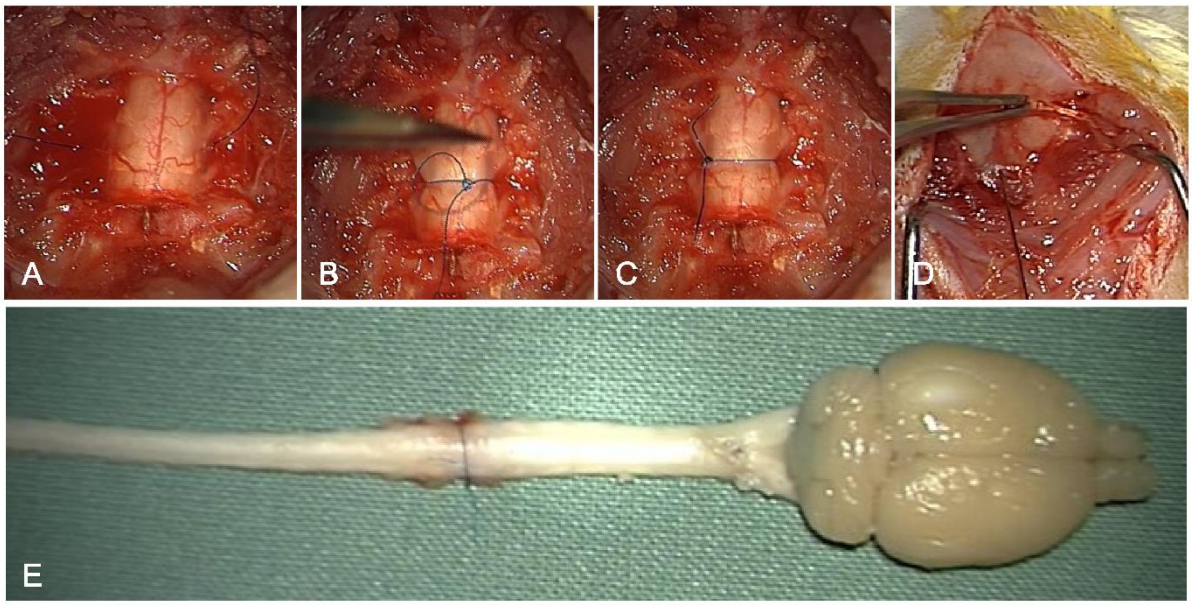

Figure 1. Surgical procedures and central nervous system dissection. (A – C) Constriction surgeries to obstruct the spinal subarachnoid space involved passing a 6-0 monofilament suture around the spinal dura mater and tightening the suture to occlude the posterior spinal vein. (D) One or six weeks post-surgery, a fluorescent CSF tracer, Alexa-Fluor 647 ovalbumin (OA-647), was injected into the cisterna magna. (E) 10 or 20 min after OA-647 injection, animals were perfused and the brain and spinal cord dissected out. The suture is between spinal levels C7 – T1.

Food and water were provided *ad libitum* and animals were monitored for signs of excessive weight loss, limb weakness, urinary retention or excessive self-grooming, all of which were treated appropriately (eg. manual expression of bladder if urinary retention was detected).

CSF tracer injection

One week or 6 weeks post-surgery time points were chosen for this study. These survival points were based on the previous finding that from 8 to 13 weeks after obstruction to CSF flow, syrinxes have been observed (Josephson *et al.*, 2001). Syrinx formation was not desired for this study, so earlier survival points were chosen. At these designated survival point, 1 or 6 weeks post-surgery, a second surgery was performed under general anaesthesia on both control and constriction animals. The cranio-cervical junction was incised at the midline to expose the atlanto-occipital membrane. Tension of the atlanto-occipital membrane was ensured by flexion of the animals' neck. Using a stereotactic micromanipulator, a 10 µL microsyringe

with a sharpened 30G needle (SGE International Pty Ltd, VIC, Australia) was inserted into the cisterna magna and retracted slightly to tent the atlanto-occipital membrane. A 5 µL injection of OA-647 (ThermoFisher Scientific, O34784, Scoresby, VIC, Australia) CSF tracer was slowly administered over 1 min into the cisterna magna. The needle was left *in situ* to prevent CSF leakage (Figure 1D). At either 10 or 20 min post-injection, the needle was withdrawn and the animal positioned supine for perfusion and fixation. The post-injection time points of 10 min and 20 min were chosen based on previous work by our group. CSF circulation of protein tracers is rapid, and beyond 20 min tracer is within peripheral lymphatic circulation.

An intracardiac injection of 2,000 IU Heparin in 400 mL ice-cold phosphate buffered saline was used for perfusion, followed by 500 mL of 4% paraformaldehyde (Lancaster Synthesis, Pelham, New Hampshire) in 0.1 M phosphate buffer (pH 7.4) at a flow rate of 50 mL/min. The spinal cord was dissected out (Figure 1E) and post-fixed in 4% paraformaldehyde in 0.1 M phosphate buffer overnight.

Immunohistochemistry

The spinal cord segments from C3 to T3 were dissected and cryoprotected in 30% sucrose solution for 48 h. Segments were embedded in Optimal Cutting Temperature compound (ProSciTech Pty Ltd, QLD, Australia) and stored at -80°C. Spinal cord segments were sectioned transversely at 40 µm on a cryostat (Leica CM 1950 Cryostat, Amtzell, Germany). Sections were thawed in a 37ºC oven for 20 min, then washed twice for 10 min in 0.01 M Tris phosphate buffered saline (TPBS, pH 7.4). The sections were then permeablised in 50% ethanol/TPBS for 20 min followed by three 10 min washes in TPBS. A blocking solution of 15% normal donkey serum (NDS)/TPBS was applied to the sections and incubated for 60 min. Sections were then treated with monoclonal anti-rat endothelial cell antibody (RECA-1, Abcam, ab9774, Melbourne, VIC, Australia) in 4% NDS/TPBS (1:100) and left overnight at 4°C. Sections were left to incubate for 2 h at room temperature, and washed twice in TPBS for 10 min. Donkey anti-mouse IgG Alexa Fluor 488 (ThermoFisher Scientific, A-21202, Scoresby, VIC, Australia) in 4% NDS/TPBS (1:400) was applied to sections for 60 min followed by two 5 min washes in TPBS. Sections were then incubated at 37ºC with monoclonal anti-actin, α-smooth muscle-Cy3 antibody (SMA-Cy3, Sigma-Aldrich, C6198, St. Louis, MO, USA) in 4% NDS/TPBS (1:400) for 30 min and twice washed in TPBS for 10 min. The sections were coverslipped with fluorescent mounting medium (DAKO, S3023, Carpinteria, CA, US) and left to dry overnight. Primary and secondary antibody exclusions were used as negative controls.

Microscopic image acquisition

A Zeiss Axio Imager Z1 microscope (Carl Zeiss Microimaging GmbH, Germany) was used to image sections. Micrograph tiles were taken at a single focal plane at 20× magnification for all three wavelength channels; SMA-Cy3, RECA-FITC and OA-647. Tri-channel micrograph tiles were stitched together to form whole spinal cord photomicrographs. Photomicrographs were acquired from C3 – T3 for quantitative image analysis. All images were taken at the same magnification and exposure times, and within a week of immunohistochemistry.

Image analysis

To assess gross tracer intensity, images were analysed using ImageJ (version 1.50i, Wayne Rasband National Institutes of Health, USA, http://imagej.nih.gov/ij/). Mean pixel values, taken as fluorescence intensities, were measured from spinal cord sections taken from C3, C7, and T1. Photomicrographs were channel split, and the OA-647 channel images were converted from RGB to 32 bit greyscale. Background was then subtracted by measuring mean pixel value of a template region of interest external to the gross spinal cord and dura. Measurements were taken of the whole spinal cord (excluding any fluorescence in the pia, arachnoid and dural layers, as well as dorsal and ventral rootlets), the whole white matter, and the whole grey matter. At least 3 replicate sections were analysed per spinal level, and the results for each spinal level were then averaged. Qualitative analysis of vessels that co-localise with OA-647 was performed on at least three replicate sections per spinal levels C3, C7 and T1. Arterioles were identified as RECA positive (RECA-positive) and SMA positive (SMA-positive) vessels. Venules were identified as RECA-positive and SMA-negative (or minimally positive), whilst capillaries were identified as RECA-positive and SMA-negative. Venules and capillaries were differentiated based on diameter; vessels equal to or greater than 6.5 µm in diameter were classified as venules; those less than 6.5 µm in diameter, capillaries. Comparisons of animal spinal cord sections within and between the same experimental or control group were made based on the location and distribution of vessels that were co-localised with OA-647. All C3, C7 and T1 spinal cord sections were assessed qualitatively for tracer localisation around vessels of identified type. Figures in this paper are representative photomicrographs and schematics of several experimental groups.

Statistical analysis

Fluorescent tracer intensity in different matter regions for control and constriction animals were compared using two-way analysis of variance (ANOVA) and adjusted for

multiple comparison using Bonferroni's post-hoc tests. Significance was taken as a p-value of less than 0.05. P-values presented in figures are group differences between control and constriction animals. Multiple comparisons reported no significant differences. All values are expressed as mean ± standard error. Excel (Microsoft, Redmond, WA, USA) and GraphPad Prism 5 (GraphPad Software, La Jolla, CA, USA) were used for data analysis.

Results

The suture tied to constrict the subarachnoid space between C7 and T1 led to occlusion of the dorsal spinal vein in all 16 animals. Animals with an extradural constriction had significant neurological deficits including hindlimb paresis and urinary retention which had resolved by 1 week post-surgery. Laminectomy-only controls showed no neurological deficits. Upon microscopic imaging, 5 constriction spinal cords showed cellular accumulation, an oedematous morphology and cavity formation all within the posterior central white matter adjacent to the central canal. There was no CSF tracer present in the damaged region. Laminectomy-only control animals did not exhibit this pathology. However, a 6 week control spinal cord from T1 to T2 had damage that was likely incurred pre-processing during the C7 – T1 laminectomy, as tracer was present in the tissue bordering the site of injury.

1 week post-surgery

Distribution of CSF tracer in the spinal cord

In control animals, the highest mean fluorescence intensities were measured in the most rostral spinal segment (C3), and the lowest mean values were measured in the more caudal segments (C7 and T1, Figure 2). In these animals, CSF tracer was primarily localised to the peripheral white matter, ventral median fissure, central canal and perivascular spaces in rostral C3 sections at both 10 and 20 min post-injection. In the caudal sections (C7 and T1), tracer was present in the ventral median fissure, central canal and perivascular spaces. Although tracer was less evident in the peripheral white matter tissue, tracer was still present around vessels.

Similar to control animals, the constriction animals had the highest mean fluorescence intensities in the rostral C3 spinal segment, and the lowest values measured in caudal C7 and T1 (Figure 2). CSF tracer was predominantly localised to the peripheral white matter of the spinal cord and in the ventral median fissure at both 10 and 20 min post-injection. The pattern of tracer localisation in the central canal was comparable to controls. CSF tracer was minimally localised to the central grey matter in control animals, and absent entirely in constriction animals.

In the 1 week post-surgery groups, no significant differences were apparent between constriction and control animals ($p > 0.05$). Although not reaching significance, white matter measurements in the 10 min post-injection constriction animals demonstrated increased tracer localisation at all three spinal segments (Figure 2A). No significant differences were observed when performing multiple comparisons using Bonferroni's post hoc test.

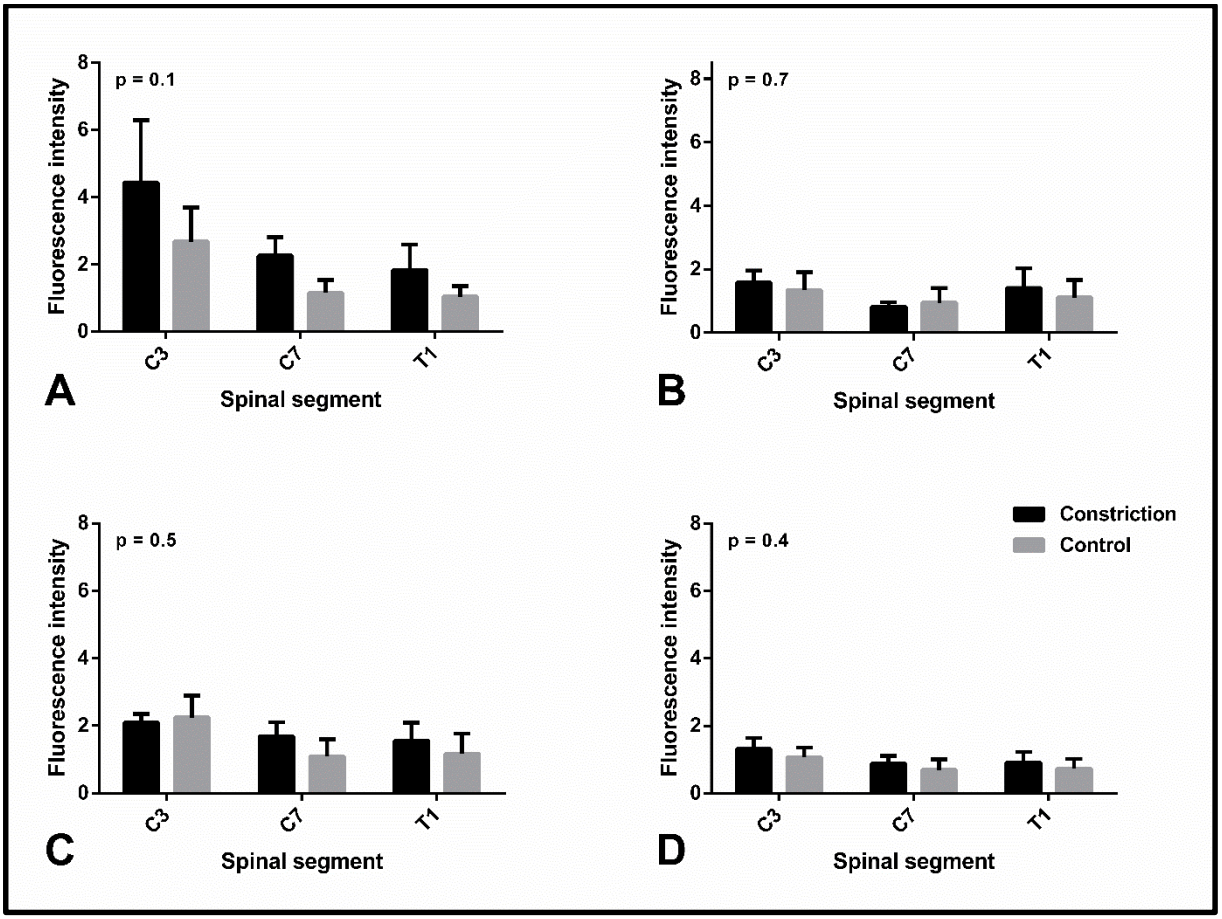

Figure 2. Quantitative measurement of CSF tracer, Alexa-Fluor 647 ovalbumin (OA-647), distribution in the white and grey matter at 1 week post-surgery. Graphs illustrate mean fluorescence intensity measured in C3, C7 and T1 spinal segments in the white matter (A, C) and grey matter (B, D) from control and constriction animals 10 min (A, B) or 20 min (C, D) post-injection of OA-647 into the cisterna magna. Results are mean pixel value ± standard error, with n = 3 for all control and constriction groups. Two-way ANOVA, p-values given.

Distribution of CSF tracer associated with blood vessels

In the 10 min post-injection control animals, CSF tracer was primarily associated with arterioles and capillaries in both grey and white matter. At 20 min post-injection in control animals, tracer predominately co-localised around capillaries, although CSF tracer was also associated with arterioles and venules. In the constriction group at both time points, the distribution of CSF tracer associated with blood vessels was highly varied between animals, and no consistent pattern could be determined.

6 weeks post-surgery

Distribution of CSF tracer in the spinal cord

Similar to the 1 week post-surgery animals, controls at 6 weeks post-surgery had the highest mean fluorescence intensities in the rostral spinal segment C3, and the lowest mean values in the more caudal spinal segments C7 and T1 (Figure 3). The CSF tracer was localised to the central canal, ventral median fissure and perivascular spaces at both 10 and 20 min post-injection. In the 10 min post-injection animals tracer was present in the central grey matter (Figure 4B), whilst in 20 min post-injection animals tracer was localised predominantly in the peripheral white matter.

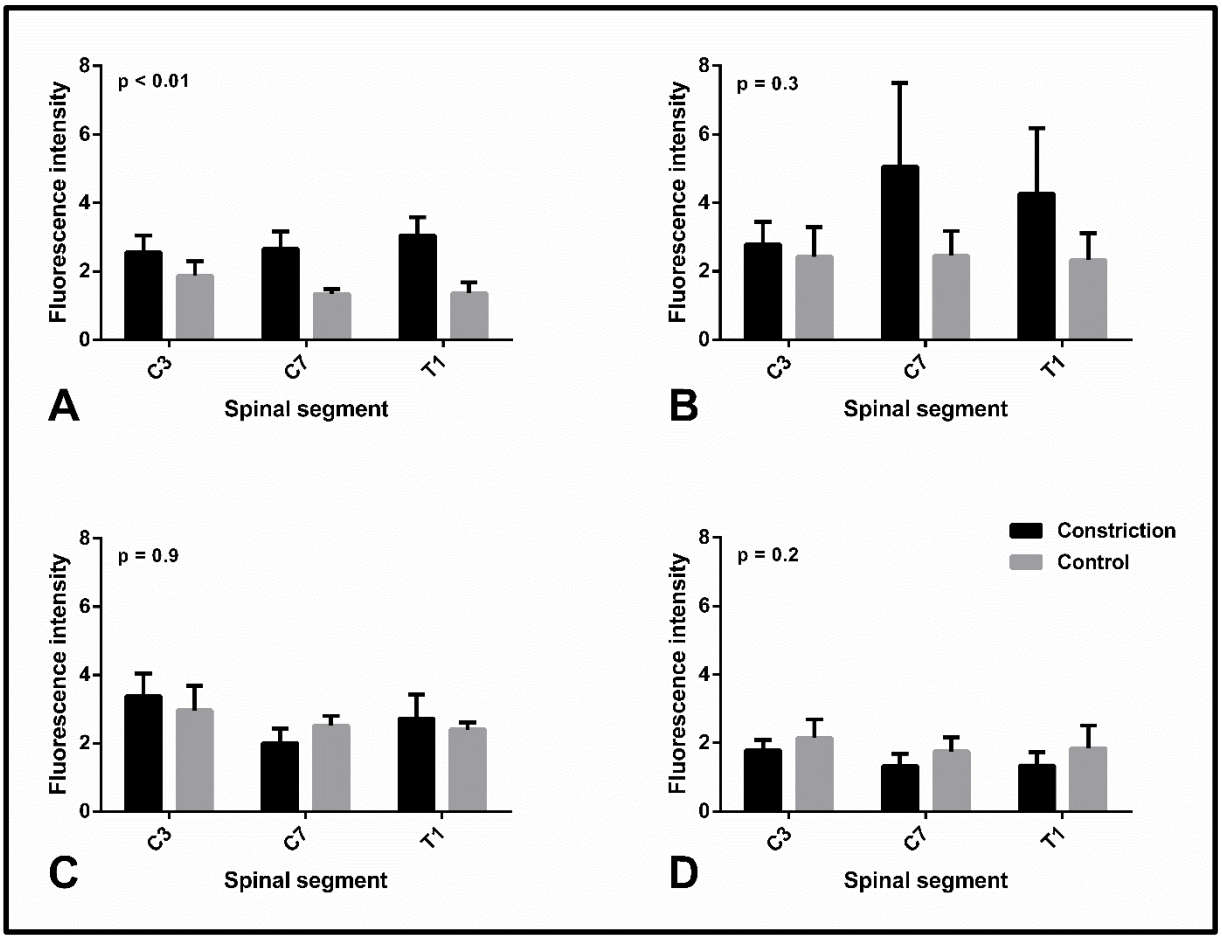

Figure 3. Quantitative measurement of CSF tracer, Alexa-Fluor 647 ovalbumin (OA-647), distribution in the white and grey matter at 6 weeks post-surgery. Graphs illustrate mean fluorescence intensity measured in C3, C7 and T1 spinal segments in the white matter (A, C) and grey matter (B, D) from control and constriction animals 10 min (A, B) or 20 min (C, D) post-injection of OA-647 into the cisterna magna. Results are mean pixel value ± standard error, with n = 3 for control groups and n = 5 for constriction groups. Two-way ANOVA, p-values given.

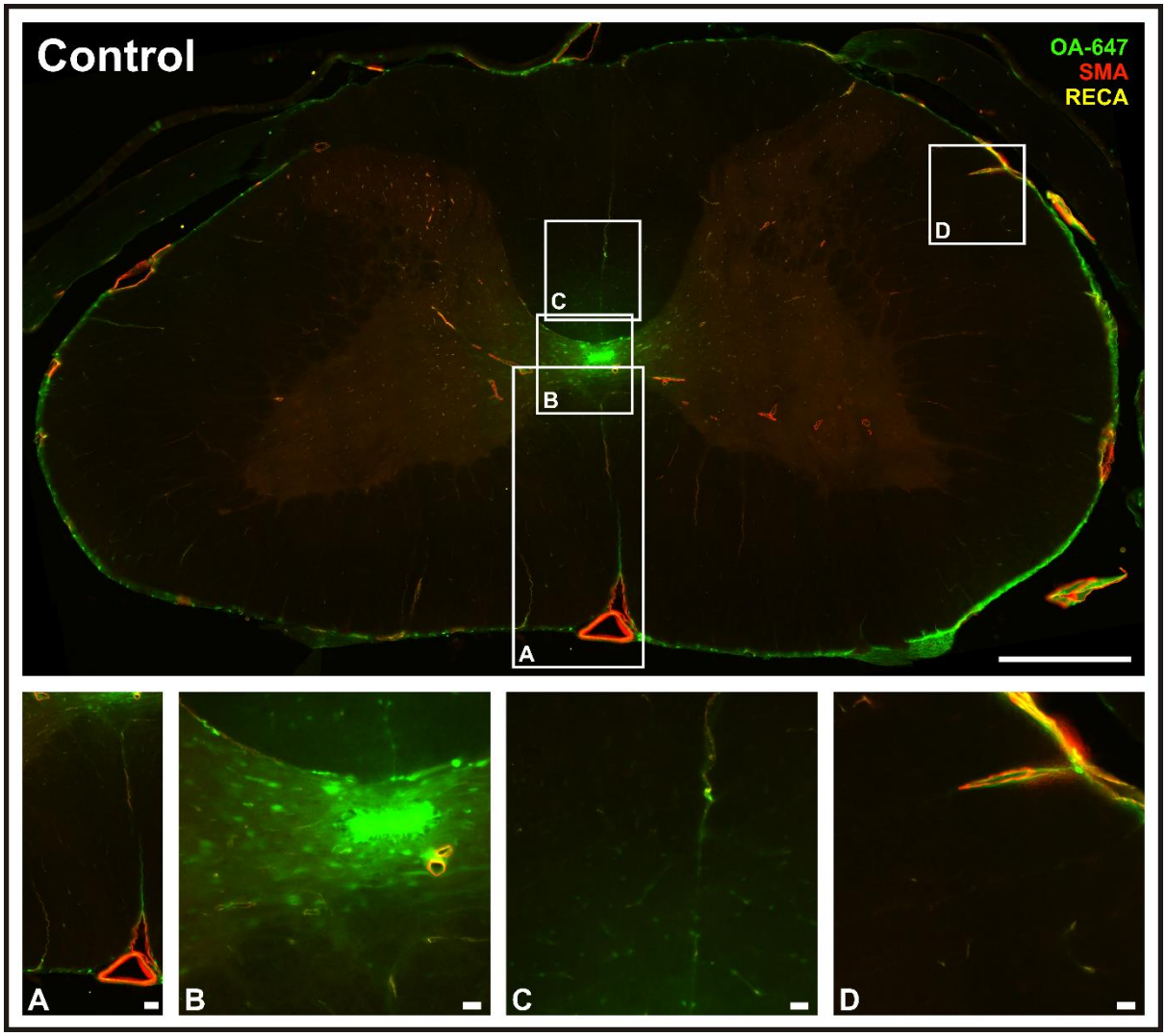

Figure 4. Microscopic imaging. Representative C7 micrographs from a control animal at 6 weeks post-laminectomy, sacrificed 10 min after injection of CSF tracer into the cisterna magna. Alexa-Fluor 647 ovalbumin (OA-647) tracer is predominantly located in the ventral median fissure (A), central canal and central grey matter (B), and the central white matter (C). The distribution of tracer in the peripheral white matter (D) was minimal compared to the central grey matter (B) and central white matter (C). All micrographs presented are merged channel images of OA-647, rat endothelial cell antigen (RECA) and smooth muscle actin (SMA). CSF tracer is co-localised around RECA-positive, SMA-positive arterioles (A, B and D) and RECA-positive, SMA-negative capillaries (C). The upper panel micrograph was taken at 20× magnification. Scale bars are 500 µm (upper panel), 50 µm (A) and 20 µm (B – D).

In constriction animals 10 min post-injection, caudal spinal segments C7 and T1 had the highest mean fluorescence intensities whilst rostral C3 had the lowest values (Figure 3A and B). In the presence of the extradural constriction, white matter measurements at 10 min post-injection demonstrated significantly higher tracer intensity ($p < 0.01$, Figure 3A). In the

same experimental group, the constriction had no significant effect on grey matter measurements (Figure 3B). However, there was a trend at C7 and T1 where the tracer intensity increased then decreased above and below the constriction respectively. CSF tracer was localised to the peripheral white matter and ventral median fissure at all three spinal segments (Figure 5A and D), with most animals also exhibiting tracer within the central canal, central grey matter and central white matter (Figure 5B and C). At 20 min post-injection, constriction animals had the highest mean fluorescence intensities at the rostral C3 spinal segment, while the lowest mean values were recorded caudally at C7 and T1 (Figure 3C and D). The mean fluorescence intensities of grey and white matter were not significantly different from controls. However, there was an increase in tracer in the white matter from C7 to T1 at the level of the constriction (Figure 3C). At all three spinal levels, CSF tracer was localised to the peripheral white matter, ventral median fissure and central canal. Using Bonferroni's post hoc test for multiple comparisons, there were no significant differences between control and constriction spinal segments.

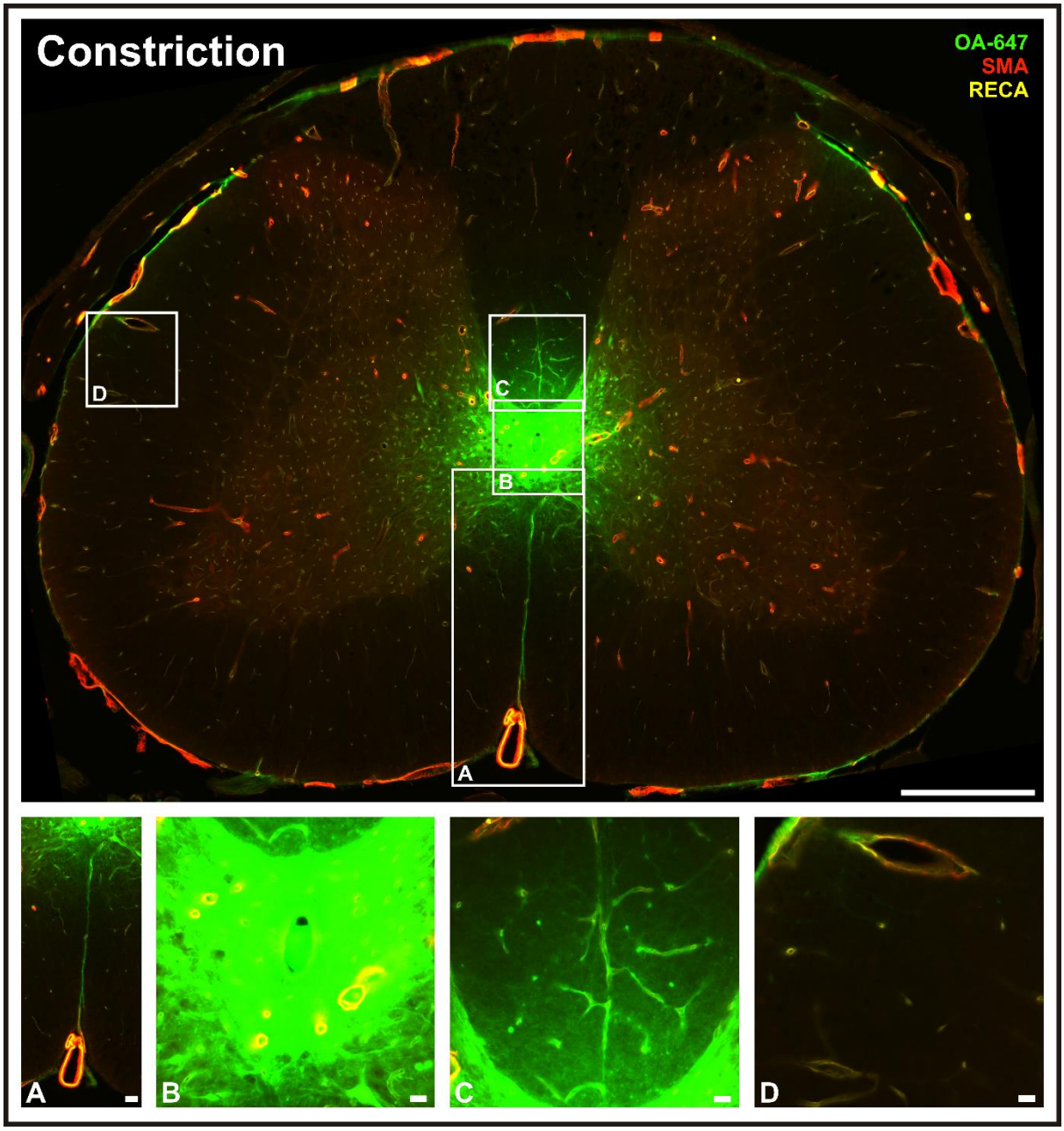

Figure 5. Microscopic imaging. Representative C7 micrographs from a constriction animal at 6 weeks post-surgery, sacrificed 10 min after injection of CSF tracer into the cisterna magna. Alexa-Fluor 647 ovalbumin (OA-647) tracer is located in the ventral median fissure (A), and extensively in the central canal and central grey matter (B) and central white matter (C). The distribution of tracer in the peripheral white matter (D) was minimal compared to the central grey matter (B) and central white matter (C). All micrographs presented are merged channel images of OA-647, rat endothelial cell antigen (RECA) and smooth muscle actin (SMA). CSF tracer co-localised around blood vessels defined as arterioles (SMA-positive, RECA-positive), capillaries (SMA-negative, RECA-positive, diameter < 6.5 µm) and venules (SMA-negative or minimally positive, RECA-positive, diameter > 6.5 µm). The upper panel micrograph was taken at 20× magnification. Scale bars are 500 µm (upper panel), 50 µm (A) and 20 µm (B – D).

Distribution of CSF tracer associated with blood vessels

In 10 min post-injection controls, tracer co-localised with arterioles near the central canal, central grey matter and peripheral white matter (Figure 6). Tracer co-localised around capillaries, predominantly in areas where CSF tracer was highly concentrated and distributed in a diffuse pattern (Figure 6A). For controls at 20 min post-injection, tracer primarily co-localised around capillaries, and to a lesser extent around arterioles at C3, C7, and T1 (Figure 7). Distribution of tracer around venules was minimal at this time point.

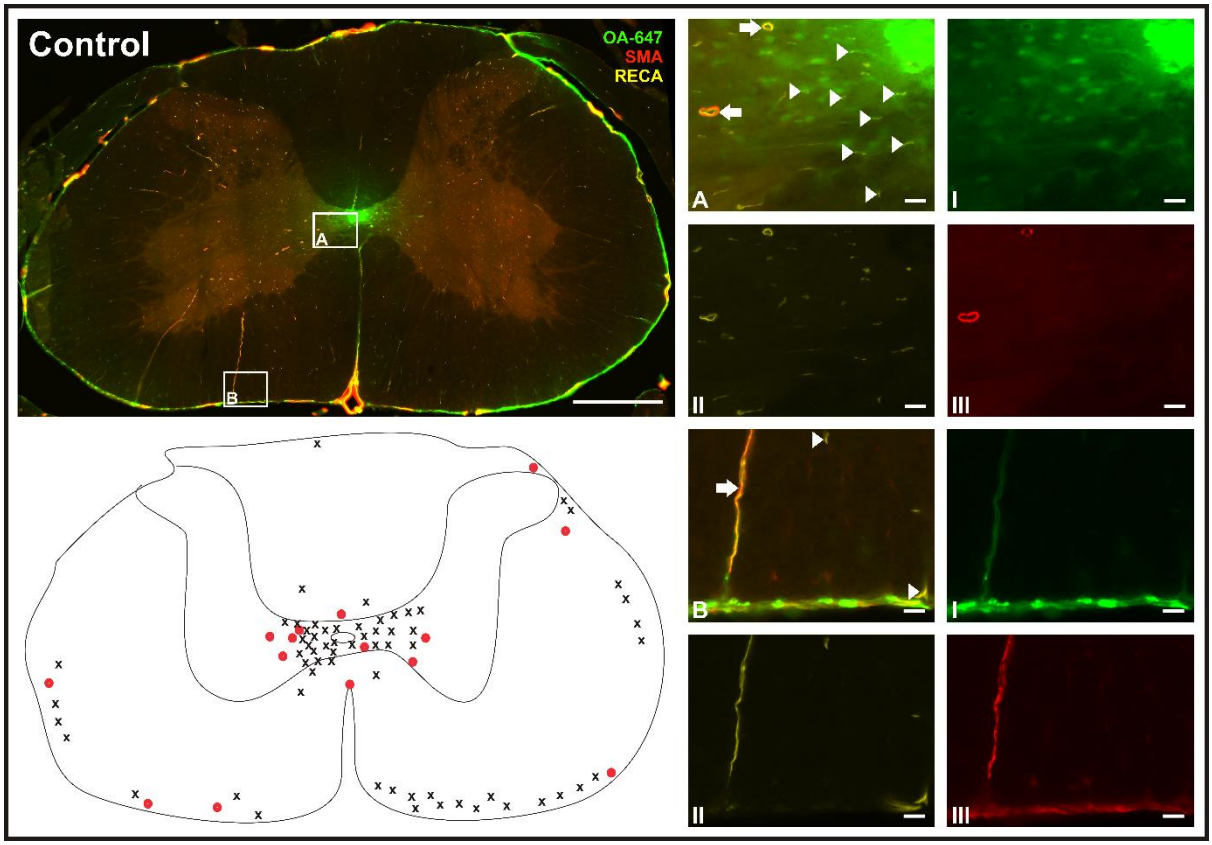

Figure 6. CSF tracer co-localisation with blood vessels. Representative T1 micrographs from a control animal at 6 weeks post-surgery, sacrificed 10 min after injection of tracer into the cisterna magna. Inset (A) of the central grey matter shows Alexa-Fluor 647 ovalbumin (OA-647) tracer localised to the central grey matter and co-localised around arterioles (arrows) and capillaries (arrowheads). Inset (B) of the peripheral white matter shows OA-647 tracer co-localised around an arteriole (arrow) and capillaries (arrowheads). Channels are split from merged insets (A) and (B) into OA-647 tracer (I), rat endothelial cell antigen (RECA, II) and smooth muscle actin (SMA, III). The lower left panel shows a schematic of a spinal cord section representing all OA-647 co-localised vessels, with SMA-positive, RECA-positive arterioles (red dots) and SMA-negative, RECA-positive capillaries, diameter < 6.5 µm (black crosses). Scale bars are 500 µm (upper left panel) and 20 µm (A and B).

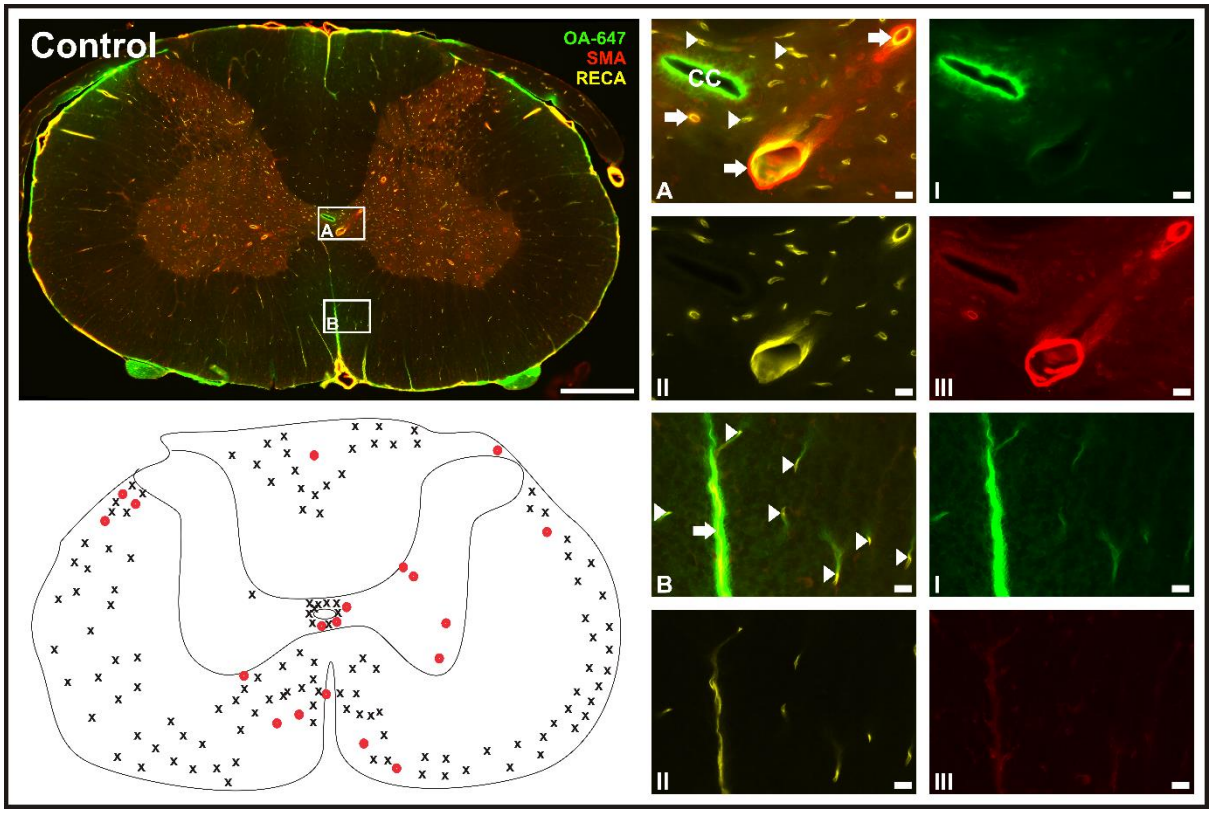

Figure 7. CSF tracer co-localisation with blood vessels. Representative C7 micrographs from a control animal at 6 weeks post-surgery, sacrificed 20 min after injection of tracer into the cisterna magna (n = 3). Inset (A) of the central grey matter shows Alexa-Fluor 647 ovalbumin (OA-647) tracer localised to the central canal (CC) and co-localised around arterioles (arrows) and capillaries (arrowheads). Inset (B) of the peripheral white matter shows OA-647 tracer localised to the ventral median fissure and co-localised around an arteriole (arrow) and capillaries (arrowheads). Channels are split from merged insets (A) and (B) into OA-647 tracer (I), rat endothelial cell antigen (RECA, II) and smooth muscle actin (SMA, III). The lower left panel shows a schematic of a spinal cord section representing all OA-647 co-localised vessels, with SMA-positive, RECA-positive arterioles (red dots) and SMA-negative, RECA-positive capillaries, diameter < 6.5 µm (black crosses). Scale bars are 500 µm (upper left panel) and 20 µm (A and B).

In the constriction group 10 min post-injection, tracer co-localised around arterioles near the central canal, central grey matter and peripheral white matter (Figure 8). However, tracer also co-localised around venules that stained RECA-positive and SMA-negative (or minimally SMA-positive) in the central grey matter and peripheral white matter (Figure 8), a finding absent in the control cohort (Figure 6). Tracer surrounded more capillaries than arterioles and venules at all three spinal levels assessed. In constriction animals at 20 min post-injection, tracer co-localised around arterioles in the central grey matter (Figure 9A and B) and peripheral white matter. Tracer also co-localised around venules in this constriction group,

yet did not follow a consistent pattern within spinal cord regions (Figure 9). Tracer co-localised around capillaries more abundantly than arterioles and venules at all three spinal levels assessed. This finding was most present in the peripheral white matter.

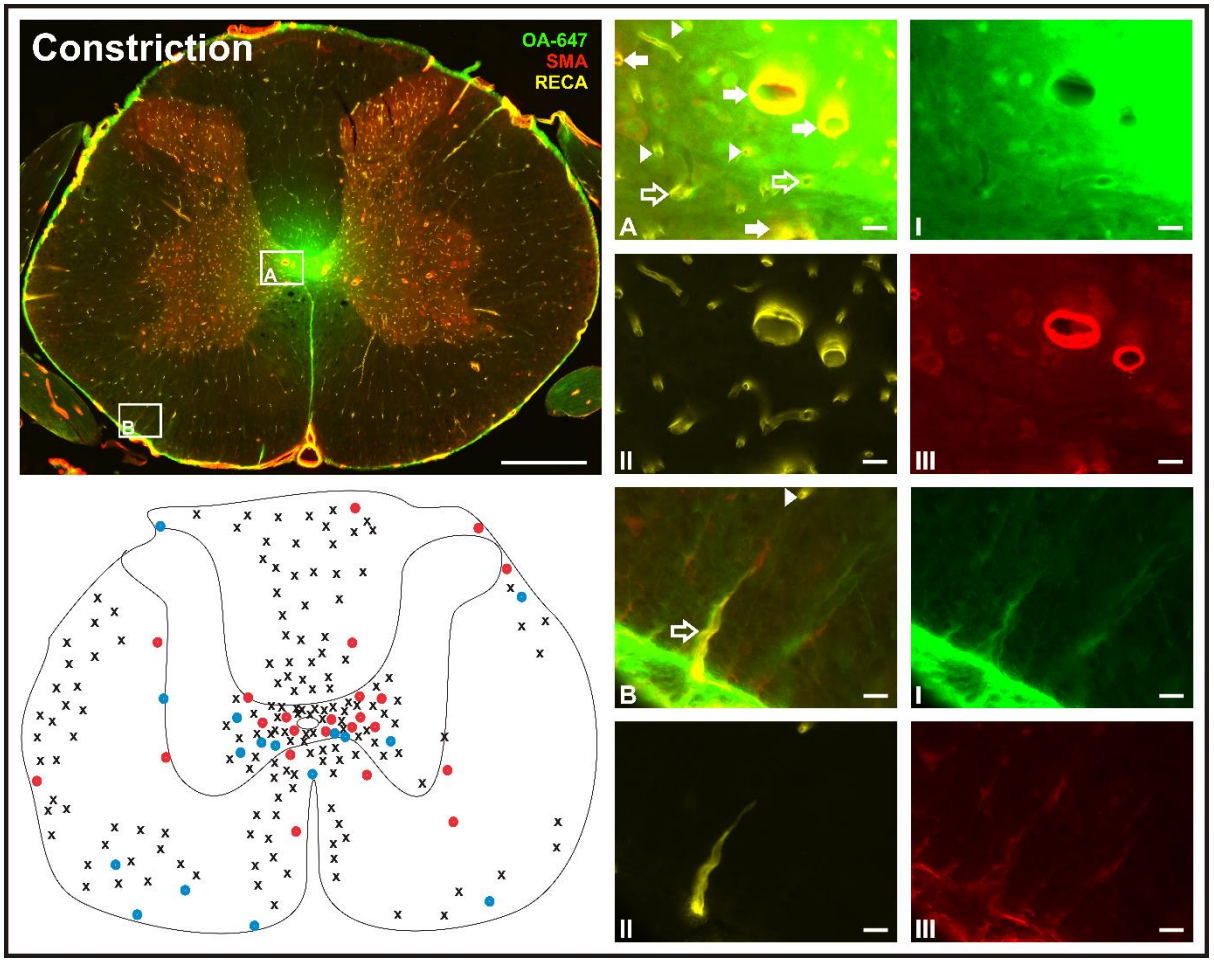

Figure 8. CSF tracer co-localisation with blood vessels. Representative T1 micrographs from a constriction animal at 6 weeks post-surgery, sacrificed 10 min after injection of tracer into the cisterna magna. Inset (A) of the central grey matter shows Alexa-Fluor 647 ovalbumin (OA-647) tracer localised to the central grey matter and co-localised around arterioles (arrows), capillaries (arrowheads) and venules (open arrows). Inset (B) of the peripheral white matter shows OA-647 tracer co-localised around a venule (open arrow) and a capillary (arrowhead). Channels are split from merged insets (A) and (B) into OA-647 tracer (I), rat endothelial cell antigen (RECA, II) and smooth muscle actin (SMA, III). The lower left panel shows a schematic of a spinal cord representing all OA-647 co-localised vessels, with SMA-positive, RECA-positive arterioles (red dots), SMA-negative, RECA-positive capillaries, diameter < 6.5 µm (black crosses) and SMA-negative (or minimally positive), RECA-positive venules, diameter > 6.5 µm (blue dots). Scale bars are 500 µm (upper left panel) and 20 µm (A and B).

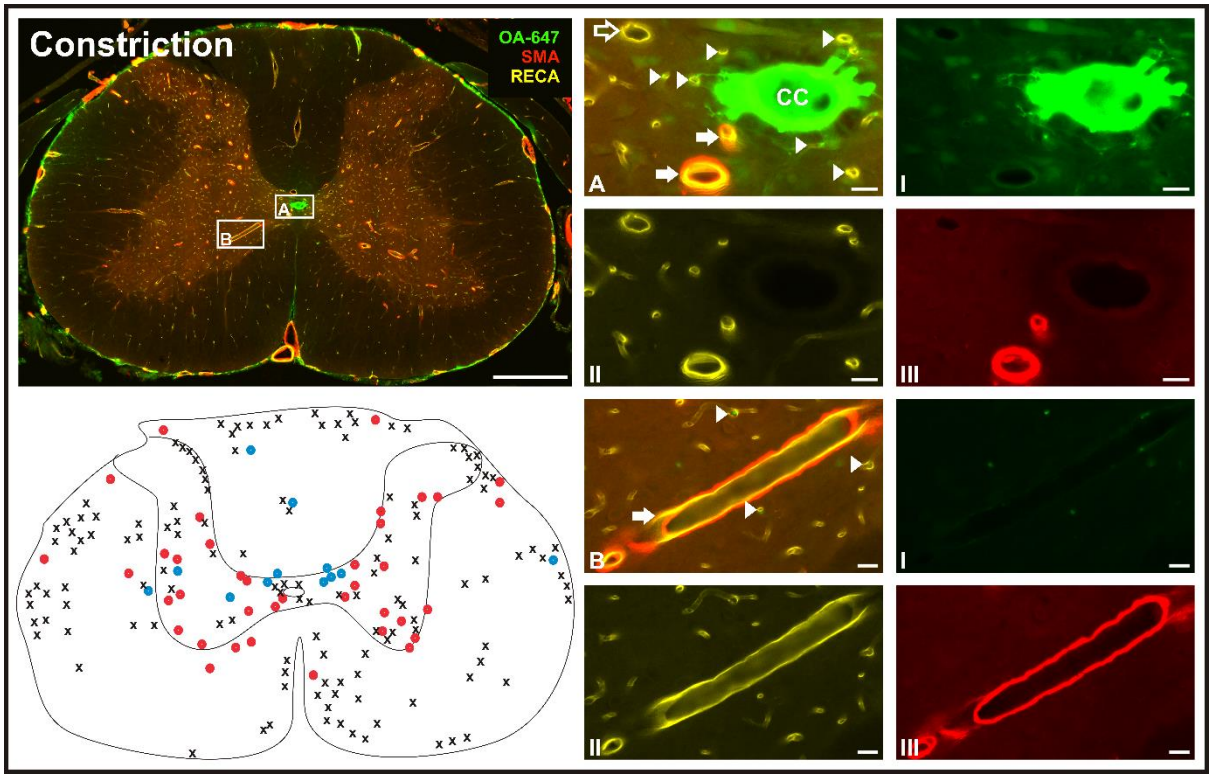

Figure 9. CSF tracer co-localisation with blood vessels. Representative C7 micrographs from a constriction animal at 6 weeks post-surgery, sacrificed 20 min after injection of tracer into the cisterna magna. Inset (A) of the central grey matter shows Alexa-Fluor 647 ovalbumin (OA-647) tracer localised to the central canal (CC) and co-localised around arterioles (arrows), capillaries (arrowheads) and a venule (open arrow). Inset (B) of the central grey matter shows OA-647 tracer co-localised around an arteriole (arrow) and capillaries (arrowheads). Channels are split from merged insets (A) and (B) into OA-647 tracer (I), rat endothelial cell antigen (RECA, II) and smooth muscle actin (SMA, III). The lower left panel shows a schematic of a spinal cord section representing all OA-647 co-localised vessels, with SMA-positive, RECA-positive arterioles (red dots), SMA-negative, RECA-positive capillaries, diameter < 6.5 µm (black crosses) and SMA-negative (or minimally positive), RECA-positive venules, diameter > 6.5 µm (blue dots). Scale bars are 500 µm (upper left panel) and 20 µm (A and B).

Discussion

The results of this study demonstrate a significant increase in CSF tracer within the white matter of animals with a subarachnoid space obstruction compared to controls at 6 weeks post-surgery, and 10 min post-injection of tracer. All other spinal cord region analyses at 6 weeks and 1 week post-surgery did not reach significance. Still, trends were present in the white matter at 1 week post-surgery, 10 min post-injection, and in the grey matter at 6 weeks post-surgery, 10 min post-injection, where CSF tracer increased in intensity at all three spinal levels of the extradural constriction animals compared to controls. In regards to the distribution of CSF tracer relative to blood vessels, control and constriction animals at 1 week and 6 weeks post-surgery showed different patterns. At 1 week post-surgery, distribution of CSF tracer was mainly found around arterioles and capillaries in both grey and white matter of controls, whilst constriction animals showed no predominant pattern of distribution. In the presence of an extradural constriction at 6 weeks post-surgery, CSF tracer co-localised around arterioles, capillaries and venules at both 10 and 20 min post-injection. The corresponding control groups showed CSF tracer co-localised around arterioles and capillaries, with few to no venules co-localised. Finally, CSF tracer located around capillaries outnumbered arterioles and venules in the control groups at 20 min post-injection. The same pattern was observed in the presence of the extradural constriction 6 weeks post-surgery, at both 10 and 20 min post-injection.

The route of fluid flow into the spinal cord is relatively unknown. CSF is generally thought to be produced primarily in the ventricular system, and from there moves into the subarachnoid space of the spinal cord where it mixes in the dense layers of arachnoid trabeculae. These sheets of delicate connective tissue convolute the bidirectional rostral-caudal flow of CSF as the CNS expands and contracts during the cardiac cycle (Feinberg and Mark, 1987, Enzmann and Pelc, 1991, Bulat and Klarica, 2011). Tortuous flow currents result, known as eddies (Haller and Low, 1971). Although the macrocirculation of CSF is generally considered bidirectional, eddies create regional microcirculations which alter the pressure gradients within the subarachnoid space (Gupta *et al.*, 2009, Gupta *et al.*, 2010). From this web of microcirculations, the flow of fluid into the spinal cord is currently thought to be via perivascular spaces. Fenestrations in the pial sheath surrounding the spinal cord allow blood vessel penetration into the parenchyma. At this superficial level, the Virchow-Robin space surrounds the penetrating blood vessel. As these vessels penetrate into the spinal cord, the enveloping pial sheath becomes more perforated to the point where pial cells exist without specialised intercellular junctions (Bulat *et al.*, 2008). Here, perivascular spaces arise as a

conduit for subarachnoid CSF. The network of fine collagen fibrils found in perivascular spaces (Zhang *et al.*, 1990) may further alter the CSF flow currents. In rats, CSF has been shown to flow from the spinal subarachnoid space into the perivascular spaces of penetrating vessels (Rennels *et al.*, 1985, Rennels *et al.*, 1990, Stoodley *et al.*, 1996). Stoodley *et al*. and Brodbelt *et al*. performed intracisternal injections of horseradish peroxidase (HRP) and found reaction product accumulating in the perivascular spaces of branches of the anterior and posterior spinal arteries, as well as in the central canal (Stoodley *et al.*, 1996, Brodbelt *et al.*, 2003b).

HRP and radiolabelled serum proteins are often used to study CSF and ISF distribution and flow patterns. Rennels *et al*. infused HRP into the cisterna magna in cats and dogs from 4 – 10 min and found that the tracer reaction product co-localised with perivascular spaces of all vessels (Rennels *et al.*, 1985). After time, micropinocytosis removed HRP reaction product across endothelial cells into the microcirculation, or into the glial cells of the cerebral parenchyma where lysosomal degradation occurred (Wagner *et al.*, 1974, Rennels *et al.*, 1985, Rennels *et al.*, 1990). Rapid influx of HRP into the perivascular space network and ingress into the interstitium has been described in the brain and the spinal cord (Rennels *et al.*, 1990, Stoodley *et al.*, 1996). More recently, Iliff *et al*. proposed that CSF flow into the cerebral cortex occurs via periarterial spaces with bulk flow across the interstitium resulting in perivenular efflux (Iliff *et al.*, 2012). However, to date no research has assessed fluid flow pathways into the spinal cord under conditions of a normal and an obstructed subarachnoid space, and whether there exists preferential flow to the perivascular spaces of a particular vessel type.

The current study suggests that subarachnoid CSF flows into spinal perivascular spaces continuously. At 6 weeks post-surgery in constriction and control animals, the pattern of tracer distribution around arterioles suggests that tracer penetrates from the ventral median fissure and branches bilaterally upon ingress to the central grey matter, or penetrates from the peripheral white matter. Iliff *et al*., after intracisternal injection of fluorescent tracers (Texas Red-dextran-3 and fluorescein isothiocyanate-dextran-2000), found that tracers preferentially flowed through the periarterial spaces of penetrating arterioles and entered the brain interstitium (Iliff *et al.*, 2012). From 5 to 30 min after injection, the smaller molecular weight tracer abundantly increased within the interstitium, suggesting that periarterial flow is a major inflow route in the brain (Iliff *et al.*, 2012). However, the extensive presence of CSF tracer around capillaries in the current study suggests that inflow of subarachnoid CSF into the spinal cord parenchyma may also continue via the basement membranes of capillaries (a pericapillary pathway). Moreover, the pattern of tracer around capillaries in the peripheral white matter in constriction

and control animals may suggest that besides the extensive transpial flow of CSF (Stoodley *et al.*, 1999), the basement membrane of capillaries is a preferential route of fluid flow into the peripheral spinal cord. However, intensely diffuse tracer present throughout the tissue could also indicate that diffusion through the pia mater or through the ependyma of the central canal is occurring. Here, tracer surrounding capillaries could suggest that tracer is crossing the basal lamina and being removed into the microcirculation. Furthermore, tracer surrounding capillaries could also indicate that fluid outflow is occurring as observed by Carare *et al*. in the brain (Carare *et al.*, 2008). A tracer study of the spinal perivascular ultrastructure may be necessary to understand whether clearance of tracer to the microcirculation is occurring, or whether the basement membrane of capillaries act as a pathway for the exchange of CSF and ISF.

It is well established that post-traumatic syringomyelia often occurs in association with CSF obstructions in the subarachnoid space (Cho *et al.*, 1994, Stoodley *et al.*, 1999, Klekamp *et al.*, 2001, Klekamp, 2002, Brodbelt and Stoodley, 2003, Brodbelt *et al.*, 2003a, Brodbelt *et al.*, 2003b, Seki and Fehlings, 2008, Kobayashi *et al.*, 2012, Wong *et al.*, 2012). Less is known about how an obstruction changes the CSF dynamics within the subarachnoid space (Bilston *et al.*, 2006, Cheng *et al.*, 2012, Stoverud *et al.*, 2013). Moreover, the effect of a subarachnoid obstruction on specific CSF flow pathways into the spinal cord has yet to be examined. In the current study significant differences were observed between control and constriction animals 6 weeks post-surgery, but not at 1 week. When the spinal subarachnoid space is under a complete, circumferential obstruction, the peak pressures within the subarachnoid space increase during the cardiac cycle, yet the CSF flow waveform is not significantly altered (Cheng *et al.*, 2012). With a partial obstruction to the subarachnoid space, the CSF flow waveform changes markedly (Cheng *et al.*, 2012). Increased CSF flow resistance due to a change in the timing of the waveform has been shown to enhance the bidirectionality of flow within the subarachnoid space (Cheng *et al.*, 2012).

By this reasoning, the extradural constriction is thought to be circumferential at 1 week post-surgery with both the suture and arachnoiditis enveloping the spinal cord at the level of the obstruction. Manipulation of the spinal cord during constriction surgery may have resulted in acute neuroinflammation within the parenchyma. This is supported by the neurological deficits observed at 1 week post-surgery. At 1 week post-surgery, the pressure differential alone within the subarachnoid space may be insufficient in altering fluid flow dynamics. By 6 weeks post-surgery, the suture and associated arachnoiditis are still thought to envelop the spinal cord.

However, the neuroinflammation is thought to have resolved as neurological deficits are minimal to none in this survival group. The constriction may be circumferential, but more convincingly may be partial at 6 weeks post-surgery. Enhanced bidirectional flow and a change in timing of the CSF flow waveform due to a partial obstruction of the subarachnoid space may distinctly alter fluid flow dynamics and may account for the enhanced fluid inflow at 6 weeks post-surgery.

In the presence of an extradural constriction at 6 weeks post-surgery, CSF tracer co-localised around arterioles, capillaries and venules at both 10 and 20 min post-injection. The corresponding control groups showed tracer co-localised with arterioles and capillaries, with few to no venules co-localised. This finding may be explained by the following: perivenular spaces act as an additional route of inflow, in conjunction with periarterial flow, in the presence of a subarachnoid obstruction; periarterial and pericapillary inflow increase in the presence of a subarachnoid obstruction to an exhaustive level, where by both 10 and 20 min post-injection CSF tracer traverses capillary basement membranes to the perivenular network; increased periarterial inflow due to the subarachnoid space obstruction results in increased outflow via perivenular spaces, or; CSF flows into periarterial spaces and the basement membrane of capillaries where it remains within the confines of the basal lamina or traverses further into the perivascular network of post-capillary venules, not entering the parenchyma at all.

Perivenular spaces may provide an additional route of inflow into the cord in the presence of a subarachnoid obstruction. Obstructions such as dorsal arachnoiditis increase CSF flow resistance in the subarachnoid space (Cheng *et al.*, 2012). Increased flow resistance and focal pressure may facilitate enhanced perivascular inflow through the theoretical pressure phase lag mechanism (Bilston *et al.*, 2010). This theory postulates that during diastole of the cardiac cycle (arterial pressure wave), perivascular spaces are at their widest. If this is the point of peak pressure in the subarachnoid space, flow resistance into the cord is at its lowest. In contrast, if the perivascular spaces are most narrow when peak subarachnoid space pressure occurs (systolic peak of the cardiac cycle), flow along perivascular spaces into the cord will face more resistance. As Bilston *et al*. hypothesised, after the systolic pulse wave passes through the subarachnoid space, higher pressure from a partial or complete obstruction may enhance flow into the dilated perivascular spaces (Bilston *et al.*, 2010). Elevated venous pressure due to increased pressure in the subarachnoid space and *vice versa* may directly increase ISF in the spinal cord (Klekamp, 2002). Influx of CSF into spinal perivascular spaces in the presence of a subarachnoid obstruction may thus occur via periarterial and perivenular routes, as indicated

by the results of this study. As such, the additional inflow of CSF into the spinal cord via perivenular spaces may cause an imbalance in CSF-ISF homeostasis, resulting in abnormal fluid accumulation.

Fluid accumulation within the spinal cord may occur in instances of subarachnoid space obstructions where fluid efflux pathways from the cord are limited. Increased subarachnoid space pressure and venous pressure (Klekamp, 2002), as well disturbances to CSF flow (Bilston *et al.*, 2010, Cheng *et al.*, 2012), may cause a disruption to perivascular outflow pathways. As CSF flow resistance in the presence of an obstruction is elevated in the subarachnoid space but not in the interstitium of the cord, fluid inflow and ISF volume increases because the two fluid spaces are not balanced (Klekamp *et al.*, 2001). As seen in the results of this study, fluid flow into the spinal cord in the presence of an extradural constriction may occur via periarterial and pericapillary pathways, and potentially via perivenular spaces. If fluid influx via periarterial and pericapillary pathways is exhausted and ISF cannot be drained effectively into the subarachnoid space (Williams, 1972, Avrahami *et al.*, 1989, Chakrabortty *et al.*, 1994), CSF tracer may traverse the basement membrane of capillaries to reach perivenular spaces. With an insufficient clearance of ISF from the spinal cord into the subarachnoid space, dilation of perivascular spaces results (Reddy *et al.*, 1989, Milhorat *et al.*, 1993, Chakrabortty *et al.*, 1994, Klekamp *et al.*, 2001). Dilation of perivascular spaces may increase CSF influx and ISF retention. Spinal ISF retention has been indicated as a progenitor to syrinx formation when spinal CSF flow is obstructed (Levine, 2004).

The ‘presyrinx state’ of fluid accumulation may potentiate further fluid influx, leading to syrinx development. If the cardiac pulse wave flowing through the network of spinal perivascular spaces is out-of-phase with the subarachnoid CSF pressure wave, there may be preferential influx of spinal CSF (Bilston *et al.*, 2010). This influx may take the route of periarterial, pericapillary or perivenular pathways, or a combination of all three. If the central canal acts a sink for the fluid and solute by-products of CSF-ISF exchange (Cserr *et al.*, 1986, Milhorat *et al.*, 1993, Milhorat *et al.*, 1994), the capacity and patency of the central canal may determine the accumulation of fluid within its confines (Storer *et al.*, 1998, Fischbein *et al.*, 1999). Moreover, if spinal perivenular spaces are the proposed fluid outflow pathway as suggested in the brain (Iliff *et al.*, 2012), obstruction to fluid outflow pathways of the cord in the presence of a subarachnoid space obstruction may further exacerbate fluid accumulation.

Limitations

Post-capillary venules were identified based on three specifications. First, venules would immunostain positive for RECA as all vessels are lined with an endothelium. Second, immunostaining should be negative, or faintly positive, for SMA due to the thin to non-existent layer of smooth muscle cells in the tunica of venules. Finally, the diametric measurement of venules would be greater than 6.5 µm based on the mean cell diameter of erythrocytes from *Rattus norvegicus* (Gregory, 2000). Based on these specifications, discrimination of venules from arterioles and capillaries was assumed plausible. However, the pericytes of capillaries and post-capillary venules have been shown to react strongly with muscle-specific anti-actin (Herman and D'Amore, 1985, Nehls and Drenckhahn, 1991). To overcome this discrepancy, future studies may adopt a different antibody that more clearly discriminates venules from other vessels. Langenkamp and Molema used an endomucin antibody for the immunohistochemical detection of vessels in the mouse brain (Langenkamp and Molema, 2009). Arterioles, labelling as endomucin-negative, were easily differentiated from endomucin-positive capillaries and venules (Langenkamp and Molema, 2009). Furthermore, endothelial cells of venules, unlike endothelial cells of capillaries, do not express an equal distribution of endomucin (Samulowitz *et al.*, 2002). This level of endothelial heterogeneity defined by endomucin, in conjunction with the SMA antibody, should definitively discriminate vessel type.

There was great variability in fluorescent intensity and tracer distribution in the spinal cord between animals within experimental groups, even in control groups. Low group n value may have greatly contributed to the trends observed not reaching significance. Increasing the number of experimental animals may prove wise for future investigations. This may allow significant interactions between control and constriction groups, as well as the effect of the constriction on spinal levels, to be observed. Even though carefully performed, the rate of injection of OA-647 CSF tracer into the cisterna magna was difficult to control. Attached to a stereotactic frame, the microsyringe of 5 µL CSF tracer was administered manually over 1 min. To manage this variable for future experiments, an automated microinjector programmed to administer tracer over a specified time frame will be implemented. Furthermore, post-surgical sacrifice of the animals is carried out supine for intracardial perfusion, which may cause CSF leakage from the cisterna magna and change tracer distribution in the subarachnoid space and spinal cord. To counter this, the femoral artery will be cannulated pre-operatively so that perfusion is carried out in the prone position with the needle still in place to prevent any CSF leakage. *In vivo* imaging of the path of tracer from the subarachnoid space into the spinal cord

would be the optimal technique of visualising fluid inflow. However, current *in vivo* technology does not meet this need. Only under complete laminectomy prior to tracer administration could the spinal inflow patterns be visualised. Even then, the efficacy of that method remains highly questionable as surrounding non-resected tissues may distort the real-time signal.

Conclusion

Homeostasis between ISF and CSF is essential for normal fluid physiology and neurological function. An increase in fluid influx *to,* or a decrease in fluid efflux *from,* the spinal cord may result in fluid accumulation and syrinx formation. The model presented in this paper is a simplified obstruction to the subarachnoid space by extradural constriction. The results support the hypothesis that flow of CSF into the spinal cord is enhanced in the presence of a subarachnoid obstruction. This increase in flow is likely to be via periarterial spaces, yet pericapillary and perivenular pathways may also be additional inflow routes. Further investigation into the role of periarterial, perivenular and pericapillary pathways for CSF flow into the spinal cord is required to draw further conclusions. With further knowledge on the fluid inflow and outflow pathways of the spinal cord, the pathogenesis of fluid accumulation pathologies such as syringomyelia will hopefully be clarified.

References

Avrahami E, Tadmor R, Cohn DF (1989) Magnetic resonance imaging in patients with progressive myelopathy following spinal surgery. J Neurol Neurosurg Psychiatry 52:176-181.

Becker DP, Wilson JA, Watson GW (1972) The spinal cord central canal: response to experimental hydrocephalus and canal occlusion. J Neurosurg 36:416-424.

Bedussi B, van Lier MG, Bartstra JW, de Vos J, Siebes M, VanBavel E, Bakker EN (2015) Clearance from the mouse brain by convection of interstitial fluid towards the ventricular system. Fluids Barriers CNS 12:23.

Bilston LE, Fletcher DF, Stoodley MA (2006) Focal spinal arachnoiditis increases subarachnoid space pressure: a computational study. Clin Biomech (Bristol, Avon) 21:579-584.

Bilston LE, Stoodley MA, Fletcher DF (2010) The influence of the relative timing of arterial and subarachnoid space pulse waves on spinal perivascular cerebrospinal fluid flow as a possible factor in syrinx development. J Neurosurg 112:808-813.

Brinker T, Stopa E, Morrison J, Klinge P (2014) A new look at cerebrospinal fluid circulation. Fluids Barriers CNS 11:10.

Brodbelt AR, Stoodley MA (2003) Post-traumatic syringomyelia: a review. J Clin Neurosci 10:401-408.

Brodbelt AR, Stoodley MA, Watling AM, Tu J, Burke S, Jones NR (2003a) Altered subarachnoid space compliance and fluid flow in an animal model of posttraumatic syringomyelia. Spine (Phila Pa 1976) 28:E413-419.

Brodbelt AR, Stoodley MA, Watling AM, Tu J, Jones NR (2003b) Fluid flow in an animal model of post-traumatic syringomyelia. Eur Spine J 12:300-306.

Bulat M, Klarica M (2011) Recent insights into a new hydrodynamics of the cerebrospinal fluid. Brain Res Rev 65:99-112.

Bulat M, Lupret V, Orehkovic D, Klarica M (2008) Transventricular and transpial absorption of cerebrospinal fluid into cerebral microvessels. Coll Antropol 32 Suppl 1:43-50.

Carare R, Bernardes-Silva M, Newman T, Page A, Nicoll J, Perry V, Weller R (2008) Solutes, but not cells, drain from the brain parenchyma along basement membranes of capillaries and arteries: significance for cerebral amyloid angiopathy and neuroimmunology. Neuropathol Appl Neurobiol 34:131-144.

Chakrabortty S, Tamaki N, Ehara K, Ide C (1994) Experimental syringomyelia in the rabbit: an ultrastructural study of the spinal cord tissue. Neurosurgery 35:1112-1120.

Cheng S, Bilston LE (2010) Computational model of the cerebral ventricles in hydrocephalus. J Biomech Eng 132:054501.

Cheng S, Jacobson E, Bilston LE (2007) Models of the pulsatile hydrodynamics of cerebrospinal fluid flow in the normal and abnormal intracranial system. Comput Methods Biomech Biomed Engin 10:151-157.

Cheng S, Stoodley MA, Wong J, Hemley S, Fletcher DF, Bilston LE (2012) The presence of arachnoiditis affects the characteristics of CSF flow in the spinal subarachnoid space: a modelling study. J Biomech 45:1186-1191.

Cheng S, Tan K, Bilston LE (2010) The effects of the interthalamic adhesion position on cerebrospinal fluid dynamics in the cerebral ventricles. J Biomech 43:579-582.

Cho KH, Iwasaki Y, Imamura H, Hida K, Abe H (1994) Experimental model of posttraumatic syringomyelia: the role of adhesive arachnoiditis in syrinx formation. J Neurosurg 80:133-139.

Cserr HF (1971) Physiology of the choroid plexus. Physiol Rev 51:273-311.

Cserr HF, Depasquale M, Patlak CS, Pullen RG (1986) Convection of cerebral interstitial fluid and its role in brain volume regulation. Ann N Y Acad Sci 481:123-134.

Davson H (1972) Dynamic aspects of cerebrospinal fluid. Dev Med Child Neurol Suppl 27:1-16.

Enzmann DR, Pelc NJ (1991) Normal flow patterns of intracranial and spinal cerebrospinal fluid defined with phase-contrast cine MR imaging. Radiology 178:467-474.

Feinberg DA, Mark AS (1987) Human brain motion and cerebrospinal fluid circulation demonstrated with MR velocity imaging. Radiology 163:793-799.

Fischbein NJ, Dillon WP, Cobbs C, Weinstein PR (1999) The "presyrinx" state: a reversible myelopathic condition that may precede syringomyelia. AJNR Am J Neuroradiol 20:7-20.

Gregory TR (2000) Nucleotypic effects without nuclei: Genome size and erythrocyte size in mammals. Genome 43:895-901.

Gupta S, Soellinger M, Boesiger P, Poulikakos D, Kurtcuoglu V (2009) Three-dimensional computational modeling of subject-specific cerebrospinal fluid flow in the subarachnoid space. J Biomech Eng 131:021010.

Gupta S, Soellinger M, Grzybowski DM, Boesiger P, Biddiscombe J, Poulikakos D, Kurtcuoglu V (2010) Cerebrospinal fluid dynamics in the human cranial subarachnoid space: an

overlooked mediator of cerebral disease. I. Computational model. J R Soc Interface 7:1195-1204.

Haller FR, Low FN (1971) The fine structure of the peripheral nerve root sheath in the subarachnoid space in the rat and other laboratory animals. Am J Anat 131:1-19.

Herman IM, D'Amore PA (1985) Microvascular pericytes contain muscle and nonmuscle actins. J Cell Biol 101:43-52.

Hladky SB, Barrand MA (2014) Mechanisms of fluid movement into, through and out of the brain: evaluation of the evidence. Fluids Barriers CNS 11:26.

Iliff JJ, Wang M, Liao Y, Plogg BA, Peng W, Gundersen GA, Benveniste H, Vates GE, Deane R, Goldman SA, Nagelhus EA, Nedergaard M (2012) A paravascular pathway facilitates CSF flow through the brain parenchyma and the clearance of interstitial solutes, including amyloid beta. Sci Transl Med 4:147ra111.

Iliff JJ, Wang M, Zeppenfeld DM, Venkataraman A, Plog BA, Liao Y, Deane R, Nedergaard M (2013) Cerebral arterial pulsation drives paravascular CSF-interstitial fluid exchange in the murine brain. J Neurosci 33:18190-18199.

Josephson A, Greitz D, Klason T, Olson L, Spenger C (2001) A spinal thecal sac constriction model supports the theory that induced pressure gradients in the cord cause edema and cyst formation. Neurosurgery 48:636-645.

Klekamp J (2002) The pathophysiology of syringomyelia - historical overview and current concept. Acta Neurochir (Wien) 144:649-664.

Klekamp J (2013) Treatment of syringomyelia related to nontraumatic arachnoid pathologies of the spinal canal. Neurosurgery 72:376-389.

Klekamp J, Volkel K, Bartels CJ, Samii M (2001) Disturbances of cerebrospinal fluid flow attributable to arachnoid scarring cause interstitial edema of the cat spinal cord. Neurosurgery 48:174-185.

Kobayashi S, Kato K, Rodriguez Guerrero A, Baba H, Yoshizawa H (2012) Experimental syringohydromyelia induced by adhesive arachnoiditis in the rabbit: changes in the blood-spinal cord barrier, neuroinflammatory foci, and syrinx formation. J Neurotrauma 29:1803-1816.

Langenkamp E, Molema G (2009) Microvascular endothelial cell heterogeneity: general concepts and pharmacological consequences for anti-angiogenic therapy of cancer. Cell and Tissue Research 335:205-222.

Levin E, Sisson WB (1972) The penetration of radiolabeled substances into rabbit brain from subarachnoid space. Brain Res 41:145-153.

Levine DN (2004) The pathogenesis of syringomyelia associated with lesions at the foramen magnum: a critical review of existing theories and proposal of a new hypothesis. J Neurol Sci 220:3-21.

Louveau A, Smirnov I, Keyes TJ, Eccles JD, Rouhani SJ, Peske JD, Derecki NC, Castle D, Mandell JW, Lee KS, Harris TH, Kipnis J (2015) Structural and functional features of central nervous system lymphatic vessels. Nature 523:337-341.

Madsen PW, 3rd, Yezierski RP, Holets VR (1994) Syringomyelia: clinical observations and experimental studies. J Neurotrauma 11:241-254.

Milhorat TH (1975) The third circulation revisited. J Neurosurg 42:628-645.

Milhorat TH, Kotzen RM, Anzil AP (1994) Stenosis of central canal of spinal cord in man: incidence and pathological findings in 232 autopsy cases. J Neurosurg 80:716-722.

Milhorat TH, Nobandegani F, Miller JI, Rao C (1993) Noncommunicating syringomyelia following occlusion of central canal in rats. Experimental model and histological findings. J Neurosurg 78:274-279.

Nakamura S, Camins MB, Hochwald GM (1983) Pressure-absorption responses to the infusion of fluid into the spinal cord central canal of kaolin-hydrocephalic cats. J Neurosurg 58:198-203.

Nehls V, Drenckhahn D (1991) Heterogeneity of microvascular pericytes for smooth muscle type alpha-actin. J Cell Biol 113:147-154.

Peraud A, Grau S (2009) Decompensated hydrocephalus causing syringomyelia and tetraparesis: a case report. Childs Nerv Syst 25:263-266.

Reddy KK, Del Bigio MR, Sutherland GR (1989) Ultrastructure of the human posttraumatic syrinx. J Neurosurg 71:239-243.

Rennels ML, Blaumanis OR, Grady PA (1990) Rapid solute transport throughout the brain via paravascular fluid pathways. Adv Neurol 52:431-439.

Rennels ML, Gregory TF, Blaumanis OR, Fujimoto K, Grady PA (1985) Evidence for a 'paravascular' fluid circulation in the mammalian central nervous system, provided by the rapid distribution of tracer protein throughout the brain from the subarachnoid space. Brain Res 326:47-63.

Saadoun S, Papadopoulos MC (2010) Aquaporin-4 in brain and spinal cord oedema. Neuroscience 168:1036-1046.

Sakushima K, Hida K, Yabe I, Tsuboi S, Uehara R, Sasaki H (2013) Different surgical treatment techniques used by neurosurgeons and orthopedists for syringomyelia caused by Chiari I malformation in Japan. J Neurosurg Spine 18:588-592.

Samulowitz U, Kuhn A, Brachtendorf G, Nawroth R, Braun A, Bankfalvi A, Bocker W, Vestweber D (2002) Human endomucin: distribution pattern, expression on high endothelial venules, and decoration with the MECA-79 epitope. Am J Pathol 160:1669-1681.

Schley D, Carare-Nnadi R, Please C, Perry V, Weller R (2006) Mechanisms to explain the reverse perivascular transport of solutes out of the brain. J Theor Biol 238:962-974.

Schurr PH, McLaurin RL, Ingraham FD (1953) Experimental studies on the circulation of the cerebrospinal fluid and methods of producing communicating hydrocephalus in the dog. J Neurosurg 10:515-525.

Seki T, Fehlings MG (2008) Mechanistic insights into posttraumatic syringomyelia based on a novel in vivo animal model. Laboratory investigation. J Neurosurg Spine 8:365-375.

Simon MJ, Iliff JJ (2016) Regulation of cerebrospinal fluid (CSF) flow in neurodegenerative, neurovascular and neuroinflammatory disease. Biochim Biophys Acta 1862:442-451.

Stoodley MA, Brown SA, Brown CJ, Jones NR (1997) Arterial pulsation-dependent perivascular cerebrospinal fluid flow into the central canal in the sheep spinal cord. J Neurosurg 86:686-693.

Stoodley MA, Gutschmidt B, Jones NR (1999) Cerebrospinal fluid flow in an animal model of noncommunicating syringomyelia. Neurosurgery 44:1065-1075.

Stoodley MA, Jones NR, Brown CJ (1996) Evidence for rapid fluid flow from the subarachnoid space into the spinal cord central canal in the rat. Brain Res 707:155-164.

Storer KP, Toh J, Stoodley MA, Jones NR (1998) The central canal of the human spinal cord: a computerised 3-D study. J Anat 192 (Pt 4):565-572.

Stoverud KH, Langtangen HP, Haughton V, Mardal KA (2013) CSF pressure and velocity in obstructions of the subarachnoid spaces. Neuroradiol J 26:218-226.

Tait MJ, Saadoun S, Bell BA, Verkman AS, Papadopoulos MC (2010) Increased brain edema in aqp4-null mice in an experimental model of subarachnoid hemorrhage. Neuroscience 167:60-67.

Torvik A, Murthy VS (1977) The spinal cord central canal in kaolin-induced hydrocephalus. J Neurosurg 47:397-402.

Wagner HJ, Pilgrim C, Brandl J (1974) Penetration and removal of horseradish peroxidase injected into the cerebrospinal fluid: role of cerebral perivascular spaces, endothelium and microglia. Acta Neuropathol 27:299-315.

Williams B (1972) Pathogenesis of syringomyelia. Lancet 2:969-970.

Wong J, Hemley S, Jones N, Cheng S, Bilston L, Stoodley M (2012) Fluid outflow in a large-animal model of posttraumatic syringomyelia. Neurosurgery 71:474-480.

Zhang ET, Inman CB, Weller RO (1990) Interrelationships of the pia mater and the perivascular (Virchow-Robin) spaces in the human cerebrum. J Anat 170:111-123.